Journal of Industrial and Engineering Chemistry 67 (2018) 92–98

Contents lists available at ScienceDirect

Journal of Industrial and Engineering Chemistry

journal homepage: www.elsevier.com/locate/jiec

Morphological transformations during drying of surfactant-nanofluid droplets

Abdulkadir Osman[a], Noushine Shahidzadeh[b], Hugh Stitt[c], Nima Shokri[a,*]

[a] School of Chemical Engineering and Analytical Science, The University of Manchester, Manchester M13 9PL, United Kingdom
[b] Institute of Physics, WZI – University of Amsterdam, Science Park 904, 1098 XH Amsterdam, the Netherlands
[c] Johnson Matthey Technology Centre, Billingham TS23 1LB, United Kingdom

ARTICLE INFO

Article history:
Received 21 May 2018
Received in revised form 11 June 2018
Accepted 20 June 2018
Available online 28 June 2018

Keywords:
Nanofluids
Droplets
Surfactants
Morphology
Drying

ABSTRACT

The effect of surfactants with different chain length on the drying dynamics of nanosized dispersion droplets and on the final morphology of the grains formed after water evaporation is investigated experimentally. An acoustic levitator was used to examine the drying dynamics of single droplets and SEM imaging was used to characterise the morphology of the final dried grains. Results show that the drying of drops with high molecular weight surfactants leads to more irregular grains and that the grain morphology is related to surface tension driven instability of the evaporating droplets which may lead to formation of hollow dried grains.

Introduction

The use of surfactants as an additive plays an important role in a variety of technological processes such as in the food industry [1], detergency [2], drug delivery [3], cosmetics [4], foam stability [5,6] and in granule formation from the drying of colloidal dispersions [7–9].

Particle formation from the drying of nanofluids has been researched extensively with the aim of controlling the drying dynamics and the characteristics of the final grains [7,10–11]. Spray drying [12] for example is a well-established process for the production of powders which typically involves the evaporation of solid–liquid droplets. The morphology of the final grains may exhibit a range of characteristics depending on the properties of the evaporating solution. Such results are a combination of various effects that strongly influences the physicomechanical processes during droplet evaporation which in turn results in different morphological transitions [13].

Several parameters have been shown to influence the grain characteristics such as the colloidal particle size [14] concentration [15] and the use of additives [16–19]. Sen et al. [14] investigated the effects of particle size and polydispersity on the morphological transitions in the drying of suspensions via spray drying. They reported that when the size and polydispersity are high, changes in the morphology occurs from sphere to doughnut shape which subsequently releases the strain formed during evaporation. Similarly, Bertrand et al. [17] investigated the effect of slurry formulation on the grain characteristics of spray dried alumina. They showed varying the properties of the evaporating solution such as the pH and the addition of binder additives significantly influences the grain shape.

The drying behaviour of single droplets have been widely investigated, providing insight into understanding the complex dynamics during phase change, as the resulting morphologies have been shown to be similar with those produced by industrial spray drying [20–29]. Walton and Mumford [20] experimentally classified, from the drying of single droplets, different types of morphology from drops containing various suspended material. In general, these were classified into skin, crystalline and agglomerated morphology which were also said to be influenced by other experimentally controllable parameters. Pauchard and Couder [21] reported the buckling of shells in the drying of latex suspension deposited on a super hydrophobic surface. Such instabilities arise as solvent evaporation from the surface leads to the formation of menisci between the primary particles which results in capillary stress [30,31]. The outer shell is capable of responding as an elastic shell and can lead to subsequent buckling of the grain [32].

* Corresponding author at: School of Chemical Engineering and Analytical Science, Room C26, The Mill, The University of Manchester, Sackville Street, Manchester M13 9PL, United Kingdom.
E-mail address: nima.shokri@manchester.ac.uk (N. Shokri).

https://doi.org/10.1016/j.jiec.2018.06.019

These instabilities have also been shown to be related to the colloidal stability of the initial suspension which has a strong influence on the drying dynamics [33–38]. Lyonnard et al. [33] investigated the effect of ionic strength and solid content of titania sols on the nanostructure and morphology formed during drying. They reported the ionic strength of the bulk solution influenced the morphology such that high and low ionic strength lead to the formation of well-defined spherical particles and irregular grains respectively. Sen et al. [34] demonstrated that the buckling instabilities during drying of droplets of the mixed colloidal suspension containing *Escherichia coli* can be arrested by tuning the surface charge on the colloidal components. The buckling is diminished as the effective repulsive stabilizing force between the colloidal particles is reduced. Similarly, Lintingre et al. [35] investigated the drying of single colloidal suspension. They showed grain deformation can be reduced by modifying the inter-particle interactions of the suspension varied through altering the ionic strength or zeta potential. Sugiyama et al. [36] examined the drying of levitated single droplets of colloidal-polymer suspension using the leidenfrost effect. They found that buckling phenomenon is influenced due to changes in the viscoelastic properties of the suspensions with high polymer molecular weight resulting in a more crumbled morphology. Acoustic levitation is another method for investigating the physics of droplet drying with no surface contact. The present authors have used evaporation of acoustically levitated droplets to demonstrate that the drying dynamics and the assembly of the final grains were influenced by the competition between diffusion and convection during drying [39]. Experimental data were expressed as a dimensionless Péclet number that enabled a characteristic diagram allowing accurate prediction of the shape of the dried colloidal droplet based on Pe.

Thus understanding the drying dynamics of colloidal dispersions as the properties of the evaporating solution changes is crucial in controlling the structures of the final dried grains. Motivated by the interest and use of additives in key industrial applications, the specific objectives of this work were to evaluate how the presence of surfactant influences the drying behaviour and the morphology of the grains obtained from silica nanosized dispersions. To do so, surfactants that belong to the same series but are distinguished by their alkyl chain length (C4, C12, and C18) were used. The drying kinetics of single droplets was examined using an acoustic levitator and scanning electron microscopy (SEM) to characterise the grains formed at the end. From the drying experiments no apparent changes were observed in the evaporation rate between pure water droplets and drops containing surfactants at the liquid–air interface. However, the morphology of the grains, from the drying of nanofluids, was significantly influenced by the surfactant molecular weight. A plausible mechanism regarding the morphological transformation of the emerging solid is illustrated.

Theoretical considerations

The accumulation of surfactants at the liquid–air interface reduces the surface tension and may influence the droplet stability [11], which in turn could impact the drying dynamics and morphology of the grains formed from nanofluid droplets. In general, the non-dimensional parameter governing the stability of the droplet interface is the Weber number, which is a measure of the relative importance of the pressure force and surface tension forces. In the case of the drying of acoustically levitated droplet, a modified Weber number, Eq. (1), is used which signifies the ratio of acoustic pressure with the stabilising surface tension forces defined as [40],

$$We = \frac{2P_0 y_0 (u_{str}/C_0)^2 R}{\sigma} \quad (1)$$

where P_0 and y_0 stand for, respectively, the atmospheric pressure and ratio of specific heats; σ is liquid–air surface tension, R is the radius of droplet, C_0 sonic velocity. The relative velocity, u_{str}, can be approximated by the acoustic streaming velocity defined as [40]

$$u_{str} = \frac{P_0 y_0 Ma}{\rho_a C_0} \quad (2)$$

The acoustic Mach number (Ma) is related to the sound pressure level, SPL, of the levitator as SPL [dB] = 193.7 + 10 log (Ma^2) (this calibration curve was provided by the manufacturer of the acoustic levitator system used in the present study which is described next).

The critical Weber number, We_c, a threshold at which the interface of fluids become unstable and leads to droplet breakup is defined as:

$$We_c = \frac{2P_0 y_0 (u_c/C_0)^2 R}{\sigma} \quad (3)$$

Droplets undergo breakup when the weber number reaches a critical value ($We > We_c$). [41] The velocity for Kelvin–Helmholtz type instability occurs when the relative motion between the levitated droplet and the surrounding air reaches a critical value, which depends on the surface tension and density of fluids calculated as [42]:

$$u_c^2 = \left[\frac{2(\rho_l + \rho_a)}{\rho_l \rho_a}\right]\sqrt{\sigma(\rho_l - \rho_a)g} \quad (4)$$

where ρ_l and ρ_a, are the density of the liquid and air respectively and g is the acceleration of gravity.

Experimental methods

An ultrasonic acoustic levitator (tec5 AG, UK) with a standard operating frequency of 58 kHz (156 dB SPL) was used to investigate the drying of single droplets and the morphology of the final grains obtained at the end of drying. The levitator consists of a reflector and a concave piezoelectric transducer. A standing wave is generated between the transducer and reflector in which a single drop can be inserted and levitated in a stationary position [43].

All of the droplet experiments were performed using deionised water in ambient conditions ($T \sim 23^\circ$ C, $RH \sim 36\%$). The study investigated spherically charge-stabilised dispersions of colloidal silica Ludox HS (Grace, ~220 m^2/g) with radius of 8 nm. The characteristics of these dispersions are reported by Goertz et al. [44]. To limit the number of variables, only the surfactant concentration was varied; the silica concentration and the initial droplet volume were kept constant at 1 wt% and 1.5 μL respectively. Anionic surfactants (Crystalline, Sigma Aldrich) were used, presented in Table 1, at concentrations of 0.1, 1, and 2 wt%. The chemical structures of the additives are shown in Fig. 1.

Anionic surfactants were selected for this study in order to minimise absorption onto the silica particles. The interaction of silica-surfactant was determined using UV–vis spectroscopy analysis based on the method described by Desarnaud et al. [45] This allows measurement of the decolourisation of a dye solution (here a cationic dye: methylene blue) due to adsorption of the dye on the oppositely charged surface (i.e. silica). The results confirmed that anionic surfactants used in this study did not adsorb on to the negatively charged surface of the silica particles, presented in Fig. 2, since the reduction of absorbance

Table 1
Surfactant used in this work.

Surfactant	Molecular formula	Molecular weight	Solubility (g/L)	CMC (wt%)
Sodium 1-butanesulfonate (BDS)	$(CH_3(CH_2)_3SO_3Na)$	160.17	368	–
Sodium dodecyl sulphate (SDS)	$(CH_3(CH_2)_{11}SO_4Na)$	288.37	10	0.23 [46,47]
Sodium 1-octadecanesulfonate (ODS)	$(CH_3(CH_2)_{17}SO_3Na)$	356.54	0.01	0.035 [48]

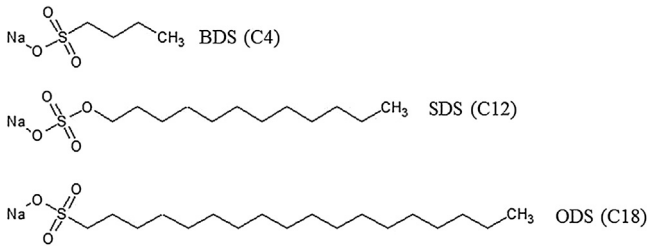

Fig. 1. Chemical structure of the anionic surfactants used in this work.

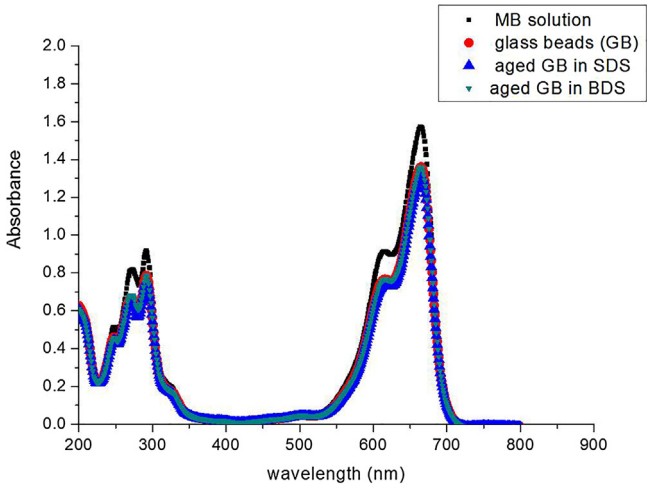

Fig. 2. UV–vis absorption spectra of methylene blue solution (MB) after the addition of silica beads and silica beads aged in BDS and SDS (0.1 wt%) solution.

(decolourisation) is almost the same when silica beads and silica beads aged in a surfactant solution are added to the methylene blue solution.

Surface tension measurements of the dispersions were carried out with K11 tensiometer (KRÜSS, Germany) employing the Du Noüy ring method which involves utilising the interaction of the platinum-iridium ring with the surface of the liquid. The measurements were repeated three times having a standard deviation under 1%.

The drops were inserted into the standing wave using a 5 μL syringe. The chamber was ventilated with a flow rate of 0.5 L/min of air during the course of the evaporation to ensure constant drying conditions [49]. An automatic imaging system was set up to record every minute the temporal evolution of the droplet during drying using a complementary metal oxide semiconductor (CMOS) camera (Canon EOS 700D). The resulting images were manually processed using ImageJ software. The aspect ratio, being the ratio between horizontal and vertical diameter, and the change in equivalent droplet diameter were calculated during drying. In particular, the cross-sectional area of the droplet, A, was computed from the images and the equivalent diameter, d, was calculated using $d = \sqrt{\frac{4A}{\pi}}$. Each experiment was repeated five times to ensure reproducibility of the data and improve statistics. The resulting dried grains were collected and subjected to SEM imaging (Quanta 200) which enabled us to investigate the morphology of the final grains as a function of the chain length and concentration of the surfactants.

Results and discussion

Surfactant effect on evaporation rate

The recorded images were used to quantify the temporal evolution of each drop as a function of the surfactant chain length and concentration (Fig. 3). The drying kinetics of droplets containing suspended particles might be divided into two stages [39]. During stage-1 drying, solvent evaporation from the surface decreases its volume and at the same time particles are transported to the surface via convective transport [50–52] which leads to the formation of a porous shell. Evaporation continues during stage-2 drying through the pores of the shell which eventually leads to typically both dry and rigid grains.

Each experiment was conducted 5 times. The standard deviation of the data for repeated experiments was small showing the technique to be robustly reproducible. In order to improve clarity, given the narrow data scatter, error bars are not shown in Fig. 3. These curves indicate that the drying behaviour of nanofluid droplets initially resembles that of pure water, i.e., a constant shrinkage of the droplet volume over time as the water evaporates. However, contrary to the case of pure water drops, water evaporation from suspensions eventually leads to the formation of dry grains. Note, in the case of droplets containing SDS surfactants (Fig. 3b and d), significant deviation in the drying dynamics during stage-1 is seen which will be explained in detail below.

The results obtained show the size of the final grain increases with increasing surfactant concentration (Fig. 3a–c). In addition, Fig. 3 also shows the effect of surfactants on the evaporation rate of water which is given as the change in droplet size over time (i.e. the slope of the line). From the drying experiments, we see that there is no apparent change in the water evaporation rate from silica-water suspensions containing surfactants, Fig. 3a–c. Additional experiments were conducted with pure water droplets and water-surfactant solution only (in the absence of suspended particles) presented in Fig. 3d. In each case, the surfactant concentrations were below its solubility in water and the drying behaviour was similar and was not influenced by the surfactant concentration or the chain length. This observation is at variance with some of literature where it is claimed that surfactant leads to retardation of the water evaporation rate [53–55]. This observation i.e., no change in the water evaporation rate in surfactant solutions is though consistent with the recent work of Qazi et al. [56].

Surfactant effect on grain morphology

Although the presence of surfactants in the dispersions had no influence on the droplet evaporation rate, various morphological transformations of the grains were observed during drying. In general, the evaporation of nanofluid droplets shrinks isotropically to form spherical grains. Fig. 4 shows the evolution of the equivalent droplet diameter and the aspect ratio (AR) over time for silica-water suspensions and those containing SDS, BDS and ODS

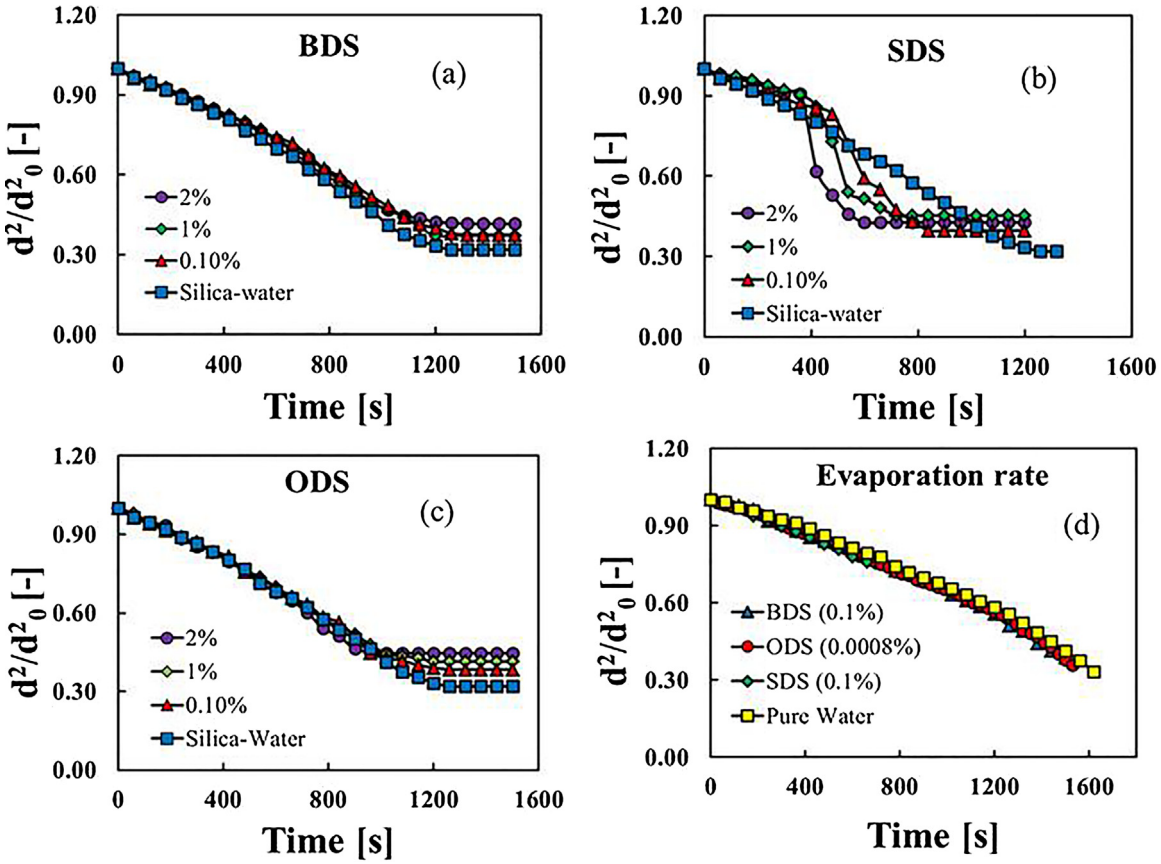

Fig. 3. The drying dynamics of droplet containing silica dispersions and surfactants of varying chain length in the case of (a) BDS (C4), (b) SDS (C12) and (c) ODS (C18). The legend indicates the initial surfactant concentration. (d) Shows the drying of pure water droplet and water + surfactant only drops.

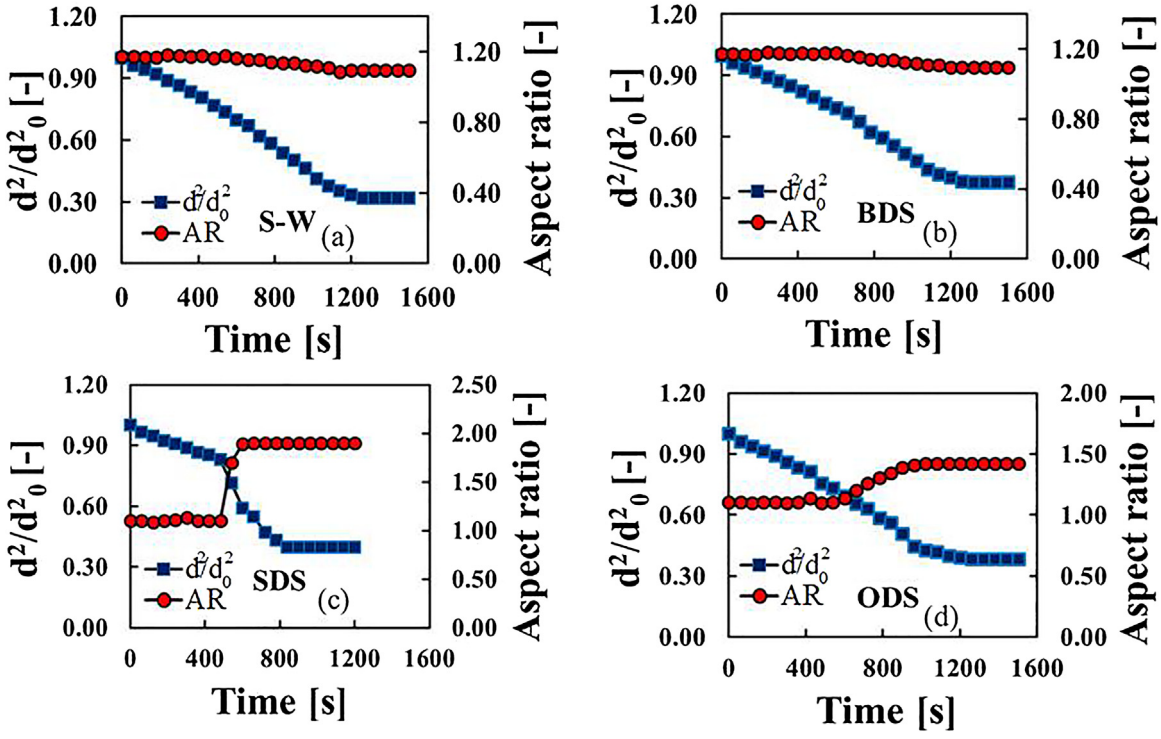

Fig. 4. Measured equivalent diameter d, and aspect ratio (AR) of (a) silica-water (SW) (b) BDS (c) SDS and (d) ODS droplets (V_0 = 1.5 μL). The surfactant concentration in all cases were 0.1 wt%.

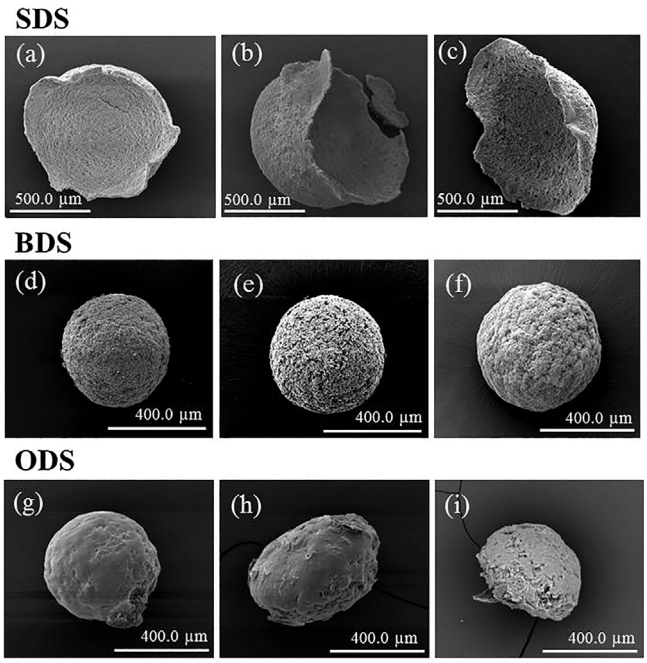

Fig. 5. SEM images of the final grains obtained from the drying of droplets of silica dispersions containing SDS (a)–(c), BDS (d)–(f) and ODS (g)–(i). In all cases, surfactants concentrations were 0.1%, 1%, and 2% (from left to right).

surfactants. Droplets tend to shrink isotropically as water evaporates. In the case of drops containing SDS however, significant deviation from sphericity was observed during the evaporation process with the AR sharply changing; see Fig. 4c. The SEM micrograph of the grain obtained from the drying of SDS nanofluid shows that a hollow morphology was typically formed, as presented in Fig. 5a–c. In contrast, silica-water suspension droplets containing BDS and ODS shrank to form solid grains i.e. grains that were not hollow.

The significant difference in the observed drying behaviour is due to breakup of the evaporating droplet in SDS-nanofluids, which led to the final dried grains exhibiting a distinct hollow morphology. This however was not seen for pure water, silica dispersions and nanofluids with BDS and ODS surfactants in which the drops remained intact throughout the drying process. Furthermore, the concentration of surfactants below and above the critical micelle concentration (Table 1) did not change the drying mechanism and the morphology of the grains as seen in Figs. 3 and 5. Although the CMC value for BDS (C4) is unknown since it is likely a hydrotrope, in any case, based on the critical micelle concentration of Sodium 1-pentanesulfonate (180 wt%) [57] which has a C5 chain length and that in general CMC increases with decreasing chain length, we can conclude that the concentrations used for BDS (0.1–2 wt%) in this study are all well below the critical micelle concentration.

As the drying dynamics are strongly associated with the addition of surfactant and its corresponding effect on the evaporating solution, surface tension measurements were conducted to see how the interfacial tension is affected. The results, presented in Fig. 6 shows a substantially lower interfacial tension in the case of SDS silica-water suspensions.

The observed behaviour indicates that droplet breakup is caused by the significant reduction in the surface tension. Using Eqs. (1) and (3) and the obtained surface tension measurements of the initial suspension presented in Fig. 6, the Weber number and critical Weber number respectively have been calculated for each case (presented in Fig. 7) to quantify the criterion for droplet atomisation. In the case of nanofluids with relatively high surface

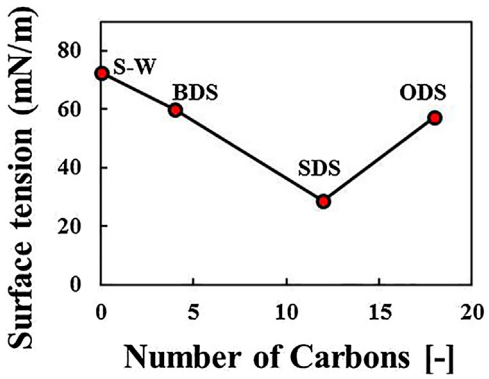

Fig. 6. Surface tension measurements of silica-water (SW) suspension and suspensions containing BDS, SDS, ODS surfactants. In all cases the surfactant concentration was 0.1 wt%.

tension, (~60–72 mNm), the droplets never reach the critical threshold at which atomisation is initiated since $We < We_c$ (Fig. 7a, b and d). At 0.1% ODS, the surface tension would not change during droplet evaporation since it is above the CMC value. Furthermore, surface tension measurements were conducted for BDS surfactant at 2% concentration which slightly reduced by ~5 mN/m compared to the measurements presented in Fig. 6. In such cases the evaporating droplets do not reach the critical threshold and therefore would shrink isotropically resulting in grains that are intact as seen in Fig. 3.

However when the droplets have a substantially lower interfacial tension the dominance of the pressure over the restoring effect of the liquid surface ultimately lead to breakage in the liquid surface. This is reflected in Fig. 7c where We is comparable to We_c at which point droplet breakup is triggered resulting in hollow grains. It is therefore evident that the instability depends on the cohesive forces of the surface layer such that the droplets can either remain intact or undergo atomisation during drying which consequently impacts the final grain morphology.

In addition, an increase in SDS concentration resulted in a slightly earlier droplet breakup exemplified by the drying curves, Fig. 3b, which was due to the formation of some foam like bubbles at higher SDS concentration (1–2%) which were not presents in the case of droplets containing 0.1% of SDS.

In the drying of droplets where breakup does not occur ($We < We_c$), such as in BDS and ODS suspensions (Fig. 7b and d), the overall shape of the final grains is influenced by the surfactant molecular weight. The drying of nanofluid droplets containing high molecular weight surfactant (C18) typically formed grains that were irregular as seen in the SEM micrographs (Fig. 5g–i). Such deviation from sphericity was not seen for nanofluid droplets with low surfactant molecular weight (C4) in which the aspect ratio (Fig. 4b), similar to silica-water suspensions (Fig. 4a), remained constant throughout the drying process to form agglomerated spherical grains. The difference in grain morphology as a function of the surfactant molecular weight is attributed to the solubility properties of the surfactants in water, Table 1. In the case of droplets containing short chain surfactants such as BDS (C4), the surfactants accumulate at the liquid–air interface to form a soluble monolayer. As evaporation proceeds, the decrease in the surface area as the droplet shrinks overtime can lead to packing and compression of the surfactant monolayer. Under compression, buckling instability can arise and result in collapse in surfactants monolayer [58–60]. Providing the surfactants are soluble, it has been shown that monolayers can relieve its surface pressure through the loss of some surfactant molecules from the interface into the aqueous phase [61]. For this reason, in the case of the drying of droplets containing BDS, we observe that the drops do

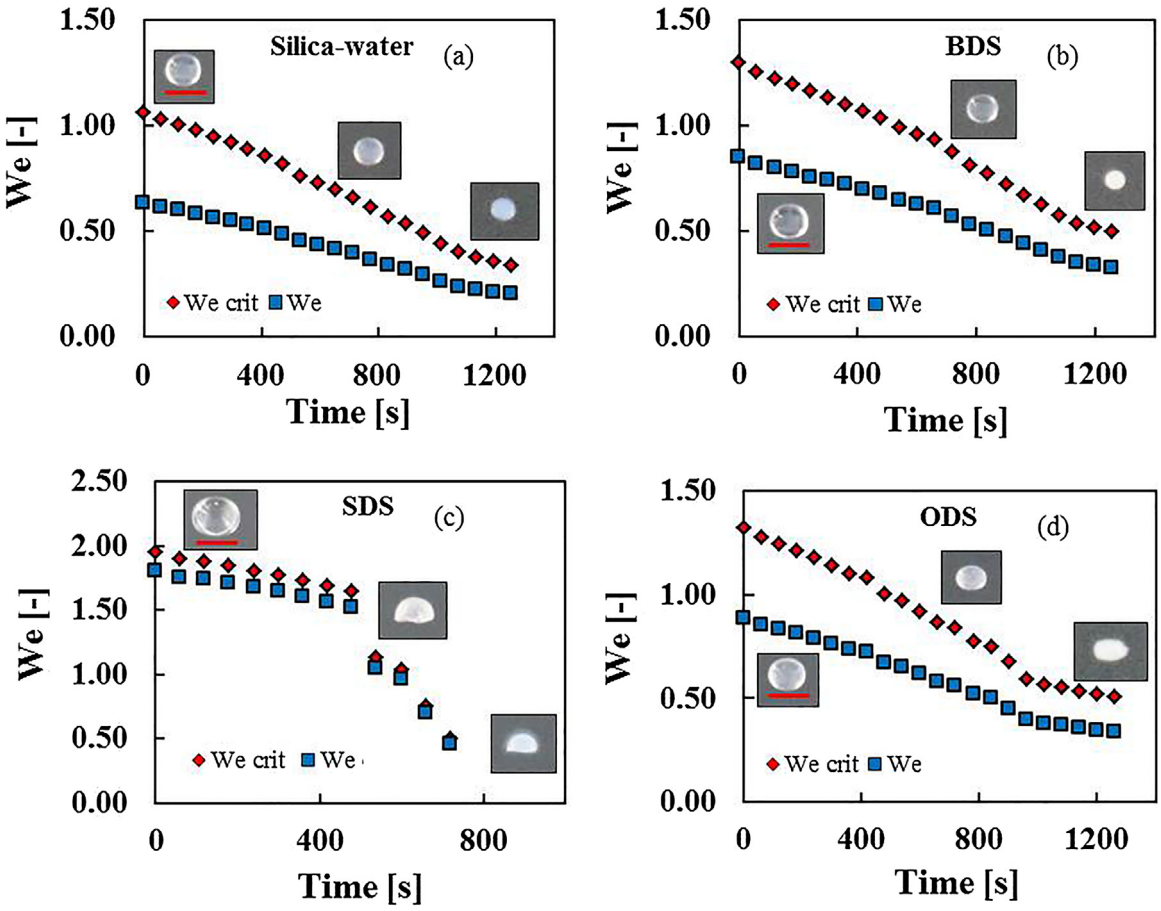

Fig. 7. Calculated Weber number (We) and critical Weber number (We_c) during drying of silica suspension in water and water + surfactants droplets (BDS, SDS and ODS at 0.1 wt%). Scale bar represent 1.5 mm.

not experience buckling (due to its high solubility) and therefore lead to the formation of spherical grains as seen in Fig. 4b. However in the case of droplets containing ODS (C18), surfactants accumulate at the surface to form relatively insoluble monolayer due to its long chains and very low solubility. In such case, as the surface area of the drops decreases during drying, the surface pressure across the monolayer is not relieved as the surfactants cannot dissolve in the aqueous phase. This eventually leads to buckling of the surfactant monolayer and subsequent deformation to the nanoparticles underneath [58], which can be seen in Fig. 4d, illustrating the deviation from sphericity as water evaporation across the surface leads to dried irregular grains. Thus, here, we show experimentally that the buckling of nanofluid droplets in the presence of surfactants can be avoided through use of surfactants with short alkyl chains.

Conclusion

The aim of the present work was to investigate the effect of surfactants that also have varying alkyl chain length (C4, C12 and C18) on the drying dynamics of silica dispersion droplets and the resulting morphology of the grains obtained at the end of the drying process. One of the main aims was to delineate parameters influencing the morphology of final particles and interpret the observed behaviour from a physical point of view without invoking any fitting parameters. To do so, single droplet drying experiments were performed using an acoustic levitator and an automatic camera to record the temporal evolution of the drying drops. From the drying experiments no apparent difference in the evaporation rate was observed between pure water droplets and drops containing surfactants. SEM imaging was used to characterise the morphology of the final dried grains obtained at the end of each experiment. It has been demonstrated that the grain morphology from the drying of nanosized dispersions can differ due to variation in the surfactant molecular weight with the resulting characteristics shown schematically in Fig. 8.

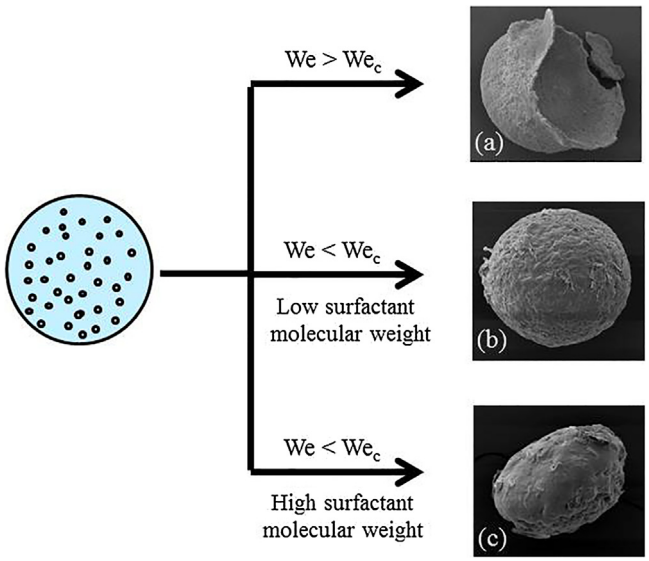

Fig. 8. A conceptual picture schematically illustrating the drying of drops under various suspension properties leading to different morphology of final grains.

Fig. 8a illustrates surface tension driven instability that results in breakup of the evaporating droplets which in turn leads to hollow dried grains. This pathway highlights the importance of the surface tension forces in maintaining stable interfaces against external forces. In contrast, when the critical threshold for atomisation is not reached ($We < We_{c)}$ and droplets remain intact, the drying behaviour and the morphology of the grains is influenced by the surfactant molecular weight, Fig. 8b–c. Droplets containing high molecular weight surfactants lead to irregular final grains. Thus, understanding the fundamental aspect of drying of droplets containing suspended particles is an essential step towards accurate production of particulate matters which is of great importance to a variety of industrial processes.

Acknowledgements

We would like to acknowledge the UK Engineering and Physical Sciences Research Council (EPSRC) to provide the PhD studentship for Abdulkadir Osman and Johnson Matthey for additional funding of this project. The authors would like to thank Alex Munnoch for insightful comments and suggestions.

References

[1] I. Kralova, J. Sjoblom, J. Dispers. Sci. 30 (2009) 1363.
[2] D.R. Karsa, Industrial Applications of Surfactants IV, The Royal Society of Chemistry, Cambridge, 1999.
[3] I. Som, K. Bhatia, M. Yasir, J. Pharm. BioAllied Sci. 4 (2012) 2.
[4] N. Kumar, R. Tyagi, Cosmetics 1 (2014) 3.
[5] K. Osei-Bonsu, P. Grassia, N. Shokri, Fuel 203 (2017) 403.
[6] K. Osei-Bonsu, N. Shokri, P. Grassia, Colloid Surf. A 481 (2015) 514.
[7] R. Vehring, W.R. Foss, D. Lechuga-Ballesteros, Aerosol. Sci. 38 (2007) 728.
[8] D.E. Walton, Dry. Technol. 18 (2000) 1943.
[9] M. Alder, M. Unger, G. Lee, Pharm. Res. 17 (2000) 863.
[10] E. Lintingre, F. Lequeux, L. Talini, N. Tsapis, Soft Matter 11 (2016) 7435.
[11] F. Iskandar, L. Gradon, K. Okuyama, J. Colloid Interface Sci. 265 (2003) 296.
[12] K. Master, Spray Drying Handbook, fifth ed., Longman Scientific & Technical, England, 1991.
[13] R. Vehring, Pharm. Res. 25 (2008) 999.
[14] D. Sen, J. Bahadur, S. Mazumder, S. Bhattacharya, Soft Matter 8 (2012) 10036.
[15] J. Bahadur, D. Sen, S. Mazumder, B. Paul, A. Khan, G. Ghosh, J. Colloid Interface Sci. 351 (2010) 357.
[16] W.J. Walker, J.S. Reed, S.K. Verma, J. Am. Ceram. Soc. 82 (1999) 1711.
[17] G. Bertrand, C. Filiatare, H. Mahdjoub, A. Foissy, C. Coddet, J. Eur. Ceram. Soc. 23 (2003) 263.
[18] O.D. Velev, A.M. Lenhoff, E.W. Kaler, Science 287 (2000) 2240.
[19] J. Bahadur, D. Sen, S. Mazumder, B. Paul, H. Bhatt, S.G. Singh, Langmuir 28 (2012) 1914.
[20] D.E. Walton, C.J. Mumford, Trans. Inst. Chem. Eng. 77 (1999) 442.
[21] L. Pauchard, Y. Couder, Europhys. Lett. 66 (2004) 667.
[22] N. Shahidzadeh, M.F.L. Schut, J. Desarnaud, M. Prat, D. Bonn, Sci. Rep. 5 (2015) 10335.
[23] S.S. Datta, H.C. Shum, D.A. Weitz, Langmuir 26 (2010) 18612.
[24] N. Fu, M.W. Woo, X.D. Chen, Dry. Technol. 30 (2012) 1771.
[25] Y. Sano, R.B. Keey, Chem. Eng. Sci. 37 (1982) 881.
[26] D.H. Charlesworth, W.R.J. Marshall, AIChE J. 6 (1960) 9.
[27] K.A. Baldwin, D.J. Fairhurst, Colloids Surf. A 441 (2014) 867.
[28] W.E. Ranz, W.R.J. Marshall, Chem. Eng. Prog. 48 (1952) 141.
[29] D.H. Shin, J.S. Allen, C.K. Choi, S.H. Lee, Langmuir 31 (2015) 1237.
[30] P.A. Kralchevsky, K. Nagayama, Langmuir 10 (1994) 23.
[31] H.S. Rabbani, V. Joekar-Niasar, N. Shokri, J. Colloid Interface Sci. 473 (2016) 34.
[32] N. Tsapis, E.R. Dufresne, S.S. Sinha, C.S. Riera, J.W. Hutchinson, L. Mahadevan, D. A. Weitz, Phys. Rev. Lett. 94 (2005) 018302.
[33] S. Lyonnard, J.R. Bartlett, E. Sizgek, K.S. Finnie, T. Zemb, J.L. Woolfrey, Langmuir 18 (2002) 10386.
[34] D. Sen, J.S. Melo, J. Bahadur, S. Mazumder, S. Bhattacharya, S.F. D'Souza, H. Frielinghaus, G. Goerigk, R. Loidl, Soft Matter 7 (2011) 5423.
[35] E. Lintingre, G. Ducouret, F. Lequeux, L. Olanier, T. Perie, L. Talini, Soft Matter 11 (2015) 3660.
[36] Y. Sugiyama, R.J. Larsen, J.-W. Kim, D.A. Weitz, Langmuir 22 (2006) 6024.
[37] C.-H. Lo, T.-M. Hu, Soft Matter 13 (2017) 5950.
[38] C. Loussert, A. Bouchaudy, J.B. Salmon, Phys. Rev. Fluids 1 (2016) 084201.
[39] A. Osman, L. Goehring, A. Patti, H. Stitt, N. Shokri, Ind. Eng. Chem. Res. 56 (2017) 10506.
[40] S. Basu, A. Saha, R. Kumar, Appl. Phys. Lett. 100 (2012) 054101.
[41] B. Pathak, S. Basu, Phys. Fluids 28 (2016) 123302.
[42] S. Chandrasekhar, Hydrodynamic and Hydromagnetic Stability, Dover Publications, New York, 1981.
[43] V. Vandaele, P. Lambert, A. Delchambre, Precis. Eng. 29 (2005) 491.
[44] V. Goertz, N. Dingenouts, H. Nirschl, Part. Part. Syst. Char. 26 (2009) 17.
[45] J. Desarnaud, D. Bonn, N. Shahidzadeh, Sci. Rep. 6 (2016) 30856.
[46] D. Yu, F. Huang, H. Xu, Anal. Methods 4 (2012) 47.
[47] A. Baran Mandal, B. Unni Nair, D. Ramaswamy, Langmuir 4 (1988) 736.
[48] Y. Moroi, Y. Izaki, M. Saito, J. Colloid Interface Sci. 149 (1992) 322.
[49] A.L. Yarin, G. Brenn, O. Kastner, D. Rensink, C. Tropea, J. Fluid Mech. 399 (1999) 151.
[50] S.M.S. Shokri-Kuehni, T. Vetter, C. Webb, N. Shokri, Geophys. Res. Lett. 44 (2017) 5504.
[51] N. Shokri, Phys. Fluids 26 (2014) 012106.
[52] N. Shokri, P. Lehmann, P. Vontobel, D. Or, Water Resour. Res. 44 (2008) W06418.
[53] J.F. Davies, R.E.H. Miles, A.E. Haddrell, J.P. Reid, Proc. Natl. Acad. Sci. U. S. A. 110 (2013) 8807.
[54] J.F. Davies, A.E. Haddrell, R.E.H. Miles, C.R. Bull, J.P. Reid, J. Phys. Chem. A 116 (2012) 10987.
[55] V.K. La Mer, Retardation of Evaporation by Monolayers, Academic Press, New York, 1962.
[56] M.J. Qazi, R.W. Liefferink, S.J. Schlegel, E.H.G. Backus, D. Bonn, N. Shahidzadeh, Langmuir 33 (2017) 4260.
[57] O. Annunziata, L. Constantino, G. D'Errico, L. Paduano, V. Vitagliano, J. Colloid Interface Sci. 216 (1999) 16.
[58] Z. Chen, M. Liu, G.Y. Liu, L. Tan, Appl. Phys. Lett. 95 (2009) 223104.
[59] W.-X. Shi, H.-X. Guo, J. Phys. Chem. B 114 (2010) 6365.
[60] S.T. Milner, J.F. Joanny, P. Pincus, Europhys. Lett. 9 (1989) 495.
[61] E. Khurana, S.O. Nielsen, M.L. Klein, J. Phys. Chem. B 110 (2006) 22136.